Discontinuous Galerkin Methods for Atmospheric Numerical Modeling

Ramachandran D Nair

(rnair@ucar.edu)

Institute for Mathematics Applied to Geosciences (IMAGe)

National Center for Atmospheric Research
Boulder, CO 80305, USA.

June 18^{th}, RPN, Montréal, Canada.

NCAR

Overview

- Motivation

Overview

- Motivation
- The Discontinuous Galerkin Method (DGM)
  1. 2D Cartesian Geometry
  2. Results
  3. Monotonic Limiting & Positivity Preservation

Overview

- Motivation
- The Discontinuous Galerkin Method (DGM)
  1. 2D Cartesian Geometry
  2. Results
  3. Monotonic Limiting & Positivity Preservation
- DGM in Spherical Geometry
  1. Cubed-Sphere Geometry (HOMME grid system)
  2. Shallow Water Model
  3. Test Results

Overview

- Motivation
- The Discontinuous Galerkin Method (DGM)
  1. 2D Cartesian Geometry
  2. Results
  3. Monotonic Limiting & Positivity Preservation
- DGM in Spherical Geometry
  1. Cubed-Sphere Geometry (HOMME grid system)
  2. Shallow Water Model
  3. Test Results
- The DG Baroclinic Model (HOMME)
  1. Vertical aspects (Lagrangian Dynamics, Remapping)
  2. Horizontal Aspects (DGM, Discretization)
  3. Results

Overview

Motivation

- Why do we need a new numerical method for discretization?
- Because, the existing methods have serious limitations to satisfy all of the following properties:
  1. Local and global conservation
  2. High-order accuracy
  3. Computational efficiency
  4. Geometric flexibility ("Local" method, AMR)
  5. Non-oscillatory advection (monotonic, positivity preservation)
  6. High parallel efficiency (Petascale capability)
- Discontinuous Galerkin Method (DGM) is a potential candidate to address all of the above issues.

Motivation: Scalability of the HOMME Framework

- **HOMME:** High-Order Method Modeling Environment relies on element-based method (spectral element (SE) or DG) and developed at CISL
- Recently, Taylor et al. (2008) have shown that the CAM/HOMME SE dynamical core scales up to 86,200 processors on an IBM BG/L (LLNL).

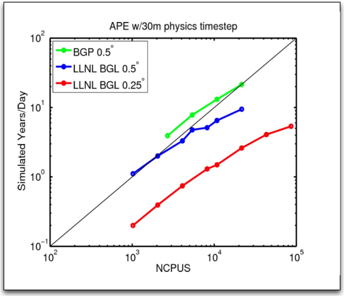

- DGM is inherently conservative, and a hybrid approach combining the best of the SE and finite-volume (FV) methods.
- DGM can handle a wide range of equations of fluid motion (compressible Euler and Navier-Stokes system *[Cockburn & Shu, 2001]*)

Flux-Form Atmospheric Equations (Conservation Laws)

- A large class of atmospheric equations of motion for compressible and incompressible flows can be written in flux (conservation) form.
- Conservation laws are systems of nonlinear partial differential equations (PDEs) in flux form and can be written:

$$\frac{\partial}{\partial t} U(\mathbf{x}, t) + \sum_{j=1}^{3} \frac{\partial}{\partial x_j} F_j(U, \mathbf{x}, t) = S(U),$$

where

  - $\mathbf{x}$ is the 3D space coordinate and time $t > 0$. $U(\mathbf{x}, t)$ is the state vector represents mass, momentum and energy etc.
  - $F_j(U)$ are given flux vectors and include diffusive and convective effects
  - $S(U)$ is the source term

- Scalar conservation law (e.g., mass continuity equation):

$$\frac{\partial \rho}{\partial t} + \nabla \cdot (\rho \mathbf{V}) = 0$$

Numerical Methods for Solving Conservation Laws: Local & Compact Methods

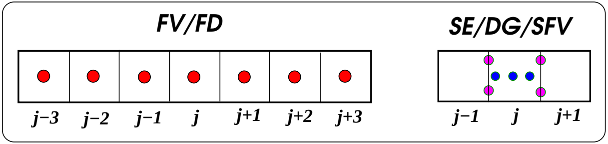

- Finite-Volume methods are traditionally used for solving conservation laws
  - E.g.: MUSCL, MPDATA, PPM, WENO, etc.
  - Computational stencil widens with order of accuracy (≥ 3)
  - Staggering is required for many applications
  - Computationally cheaper compared to the high-order methods on serial computers
  - Parallel communication "bottleneck" with high-order (petascale capable?)
- Local and Compact high-order methods
  - E.g: SE, DG, spectral finite-volume (SFV), SFD, etc..
  - Truly local, computational stencil remains the same with increasing order
  - Expensive methods on serial computers (more d.o.f per element)
  - No staggering. Cost-effective with moderate order (3^{rd} or 4^{th})
  - Excellent Parallel efficiency

Discontinuous Galerkin (DG) Methods in 2D Cartesian Geometry

2D Scalar conservation law:

$$\frac{\partial U}{\partial t} + \nabla \cdot \mathbf{F}(U) = S(U), \quad \text{in} \quad (0, T) \times \mathcal{D}; \quad \forall\, (x^1, x^2) \in \mathcal{D},$$

where $U = U(x^1, x^2, t)$, $\nabla \equiv (\partial/\partial x^1, \partial/\partial x^2)$, $\mathbf{F} = (F, G)$ is the flux function, and S is the source term.

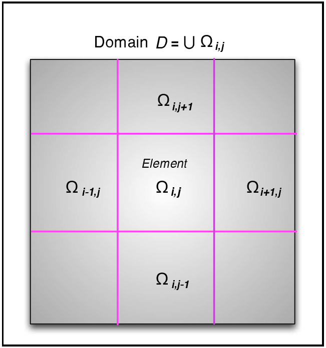

- The domain $\mathcal{D}$ is partitioned into non-overlapping elements Ω_{ij}
- Element edges are discontinuous
- Problem is locally solved on each element Ω_{ij}

DG-2D Spatial Discretization for an Element Ω_e in $\mathcal{D}$

- Approximate solution U_h belongs to a vector space $\mathcal{V}_h$ of polynomials $\mathcal{P}_N(\Omega_e)$.
- The Galerkin formulation: Multiplication of the basic equation by a *test function* $\varphi_h \in \mathcal{V}_h$ and integration over an element Ω_e with boundary Γ_e,

$$\int_{\Omega_e} \left[\frac{\partial U_h}{\partial t} + \nabla \cdot \mathbf{F}(U_h) - S(U_h) \right] \varphi_h d\Omega = 0$$

- Weak Galerkin formulation : Integration by parts (Green's theorem) yields:

$$\frac{\partial}{\partial t} \int_{\Omega_e} U_h \, \varphi_h \, d\Omega - \int_{\Omega_e} \mathbf{F}(U_h) \cdot \nabla \varphi_h \, d\Omega \quad + \int_{\Gamma_e} \mathbf{F}(U_h) \cdot \vec{n} \, \varphi_h \, d\Gamma = \int_{\Omega_e} S(U_h) \, \varphi_h d\Omega$$

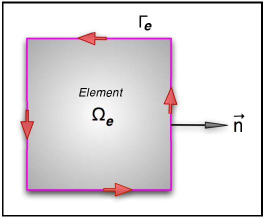

- Orthogonal polynomials (basis functions) are employed for approximating U_h and φ_h on Ω_e.
- Surface and line integrals are evaluated with high-order Gaussian quadrature rule
- Exact Integration: The flux (line) integral should be an order higher than the surface integral *(Cockburn & Shu, 1989)*.

DG-2D: High-Order Nodal Spatial Discretization

- The nodal basis set is constructed using a tensor-product of Lagrange polynomials $h_i(\xi)$, with roots at Gauss-Lobatto-Legendre (GLL) quadrature points $\{\xi_i\}$.

$$h_i(\xi) = \frac{(\xi^2 - 1)\, P'_N(\xi)}{N(N+1)\, P_N(\xi_i)\, (\xi - \xi_i)}; \quad \int_{-1}^{1} h_i(\xi) h_j(\xi) \simeq w_i \delta_{ij}.$$

- $P_N(\xi)$ is the N^{th} degree Legendre polynomial; and w_i are Gauss quadrature weights

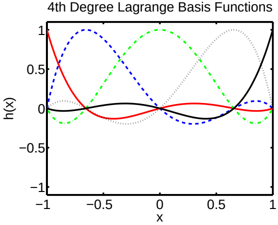

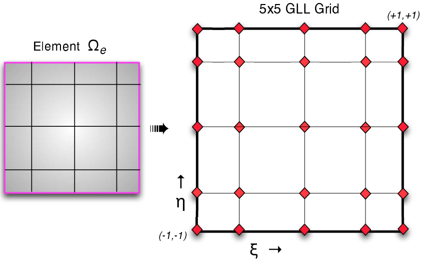

The approximate solution U_h and test function are represented in terms of nodal basis set.

$$U_{ij}(\xi,\eta) = \sum_{i=0}^{N}\sum_{j=0}^{N} U_{ij}\, h_i(\xi)\, h_j(\eta) \quad \text{for} \quad -1 \le \xi,\eta \le 1,$$

DG-2D: The Flux Term

Resolving the discontinuity at element edges by numerical flux

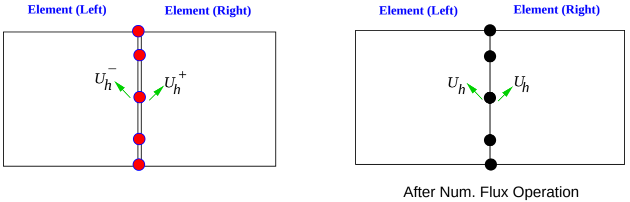

- Along the boundaries (Γ_e) of the element Ω_e the solution U_h is discontinuous (U_h^- and U_h^+ are the left and right limits).
- Therefore, the analytic flux $\mathbf{F}(U_h) \cdot \vec{n}$ must be replaced by a numerical flux such as the Lax-Friedrichs Flux:

$$\mathbf{F}(U_h) \cdot \vec{n} = \frac{1}{2} \left[(\mathbf{F}(U_h^-) + \mathbf{F}(U_h^+)) \cdot \vec{n} - \alpha (U_h^+ - U_h^-) \right].$$

- Note: For scalar problem $\alpha = \max |F'(U)|$, and for a system α is the upper bound on the absolute value of eigenvalues of the flux Jacobian $\mathbf{F}'(U)$.

DGM: Explicit Time Integration Method

- Final form for the discretization leads to an ODE for each $U_{ij}(t)$;

$$\frac{d}{dt} U_{ij}(t) = \frac{4}{\Delta x_i^1 \Delta x_j^2 \, w_i w_j} \, [I_{Grad} + I_{Flux} + I_{Source}]$$

- For a system of conservation laws, solve the decoupled ODE system:

$$\frac{d}{dt} U_h(t) = \mathcal{L}(U_h) \quad \Rightarrow \quad \frac{d}{dt} \mathbf{U}_h = L(\mathbf{U}_h) \quad \text{in} \quad (0, T)$$

- Strong Stability Preserving third-order Runge-Kutta (SSP-RK) scheme (*Gottlieb et al., SIAM Review, 2001*)

$$\begin{aligned}
U^{(1)} &= U^n + \Delta t \mathcal{L}(U^n) \\
U^{(2)} &= \frac{3}{4} U^n + \frac{1}{4} U^{(1)} + \frac{1}{4} \Delta t \mathcal{L}(U^{(1)}) \\
U^{n+1} &= \frac{1}{3} U^n + \frac{2}{3} U^{(2)} + \frac{2}{3} \Delta t \mathcal{L}(U^{(2)}).
\end{aligned}$$

where the superscripts n and $n+1$ denote time levels t and $t + \Delta t$, respectively

The DG, SE & FV Methods

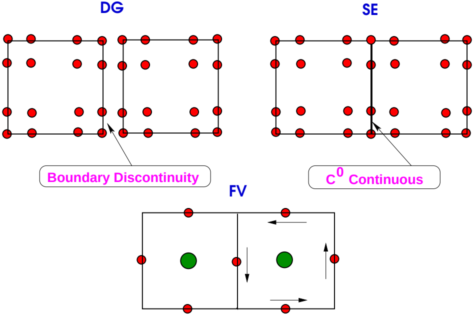

- For DGM degrees of freedom *(d.o.f)* to evolve per element is N^2, where N is the order of accuracy.
- For FV method the *d.o.f* is 1 (cell-average), irrespective of order of accuracy.
- DGM is based on conservation laws but exploits the spectral expansion of SE method and treats the element boundaries using FV "tricks."

DG-2D Advection Test: Solid-Body Rotation of a Gaussian-Hill

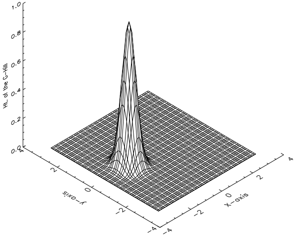

- *h*-error: Keep the degree of the polynomial fixed, change number of elements
- *p*-error: Keep the number of elements fixed, change degree of polynomial
- Spectral convergence

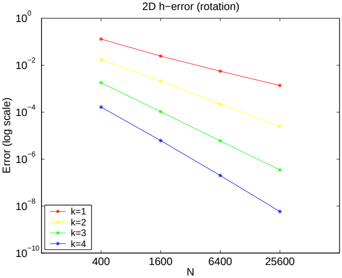

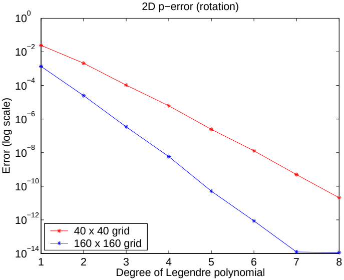

DG-2D: Scaling Results (Levy, Nair & Tufo, 2007)

- Problem: Advection of a Gaussin-hill, 80 $\times$ 80 elements with 6 $\times$ 6 GLL grid
- Strong scaling is measured by increase the number processes running while keeping the problem size constant
- Weak scaling is measured by scaling the problem along with the number of processors, so that work per process is constant

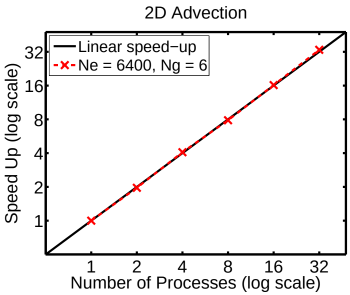

Strong scaling

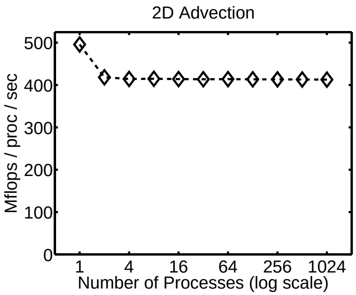

Weak scaling

DG Explicit time integration: CFL Stability

- High-order Galerkin methods have stringent explicit time-stepping limitation
- The Courant number (CFL) for the DG scheme is estimated to be $1/(2k+1)$, where k is the degree of the polynomial (*Cockburn and Shu, 1989*).
- For a third-order Runge-Kutta time stepping estimated CFL (Cockburn & Shu, 2001):

Degree (k):	1	2	3
CFL:	0.409	0.209	0.130

- Remedy: Use low-order polynomials ($k \leq 3$) or efficient semi-implicit / implicit time integrators
- Efficient time integration schemes for DG methods are under investigation (on going research under DOE SciDAC project)

Monotonic Limiter for DG transport

- Importance:
  - In atmospheric models, mixing ratios of the advecting chemical species and humidity should be non-negative and free from spurious oscillation.
  - The model should avoid creating unphysical negative mass
- Challenges:
  - Godunov theorem (1959): "Monotone scheme can be at most first-order accurate"
  - There is a "conflict of interest" between the high-order methods and monotonicity preservation!
  - In principle, a limiter should eliminate spurious oscillation and preserve high-order nature of the solution to a maximum possible extent
- Existing Limiters for DGM:
  - Minmod limiter (Cockburm & Shu, 1989): Based on van Leer's slope limiting, but too diffusive
  - Limiters based on WENO (Qui & Shu 2005), Moments (Krivonodova, 2008): Expensive and no positivity preservation

DG-2D: A New Limiter for Transport Problems

- The minmod limiter can be applied in x and y-direction sequentially, however it is very diffusive.

$$U_h(x,y,t) = \overline{U}_h(t) + U_x(t)\,x + U_y(t)\,y + U_{xy}(t)xy + U_{xx}(t)x^2 + U_{yy}(t)y^2 + \mathrm{HOT}$$

- First, check for the positivity violation of $U_{xy}(t)$, $U_{xx}(t)$ and $U_{yy}(t)$. If necessary, limit the low-order terms $U_x(t)$ and $U_y(t)$.

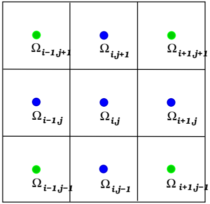

- Limiter selectively applies slope limiting employs a 3×3 element stencil and positivity as a constraint. The resulting method is up to third-order accurate.

DG-2D $\mathcal{P}^2$ (Third-Order): Solid-Body Rotation (Leveque, 2004)

Solid-Body rotation of a cosine-cone and a square block (80 $\times$ 80 elements, 3 $\times$ 3 GLL points)

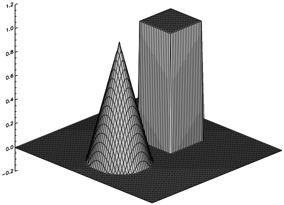

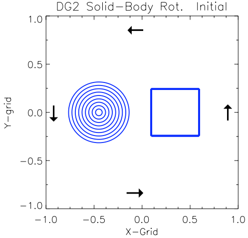

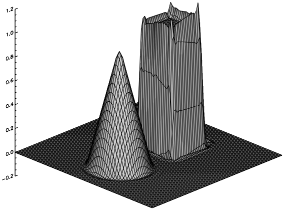

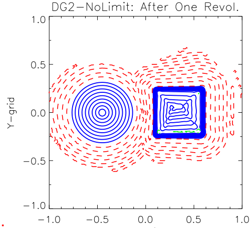

After one revolution, no limiting

DG2D: Monotonic limiting (with positivity preservation)

Solid-Body rotation after one revolution with constrained limiting

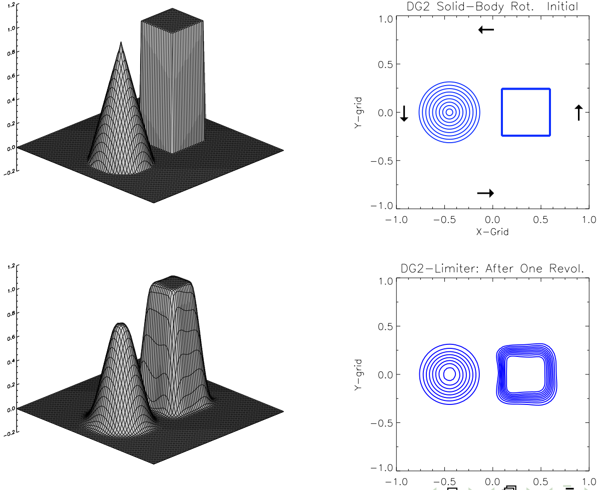

Extending DG Methods to Spherical Geometry

The Cubed-Sphere Topology *[Sadourny, MWR 1972]*

- Free of polar singularities
- Quasi-uniform rectangular mesh
- Non-orthogonal grid lines, discontinuous edges
- Well suited for the element-based methods such as DG or SE

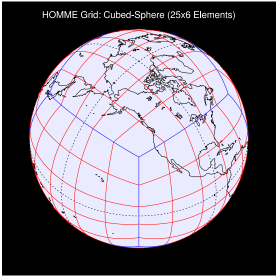

Cubed-Sphere: Central (Gnomonic) Projection

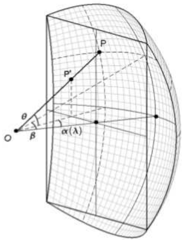

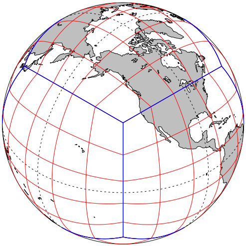

- The sphere is decomposed into 6 identical regions, using the central (gnomonic) projection of an inscribed cube with side $2a$:
  - Equiangular projection using central angles $\alpha, \beta \in [-\pi/4, \pi/4]$, $(\Delta\alpha = \Delta\beta)$
  - Equiangular projection generates more uniform mesh on the sphere as opposed to equidistant projection [*Rancic et al., 1996; Nair et al. 2005*]
  - All the grid lines are great-circle arcs

Non-Orhogonal Cubed-Sphere Grid System

Metric Tensor G_{ij}, [Cubed-Sphere $\rightleftharpoons$ Sphere] Transform

Central angles $(\alpha, \beta) = (x^1, x^2)$ are the independent variables such that $x^1, x^2 \in [-\pi/4, \pi/4]$.

$$G_{ij} = \frac{R^2}{\rho^4 \cos^2 x^1 \cos^2 x^2} \begin{bmatrix} 1 + \tan^2 x^1 & -\tan x^1 \tan x^2 \\ -\tan x^1 \tan x^2 & 1 + \tan^2 x^2 \end{bmatrix}$$

where $\rho^2 = 1 + \tan^2 x^1 + \tan^2 x^2$, $i, j \in \{1, 2\}$

Computational domain is the cube $[-\pi/4, +\pi/4]^3$

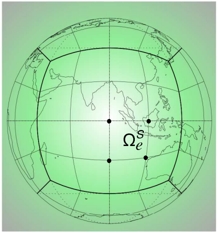

Physical Domain

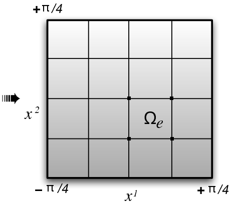

Computational Domain

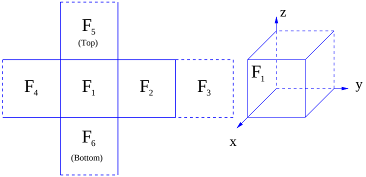

Cubed-Sphere Geometry in terms of Regular (λ, θ) Coordinates

Metric tensor in terms of longitude-latitude (λ, θ):

$$G_{ij} = A^T A; \quad A = \begin{bmatrix} R\cos\theta\,\partial\lambda/\partial x^1 & R\cos\theta\,\partial\lambda/\partial x^2 \\ R\,\partial\theta/\partial x^1 & R\,\partial\theta/\partial x^2 \end{bmatrix}$$

- The Jacobian of the transformation (metric term) is

$$\sqrt{G} = [\det(G_{ij}]^{1/2}$$

- The matrix A is used for transforming spherical (physical) velocity (u, v) to the covariant (u_1, u_2) and contravariant (u^1, u^2) velocity.

$$\begin{bmatrix} u \\ v \end{bmatrix} = A \begin{bmatrix} u^1 \\ u^2 \end{bmatrix}; \quad G^{ij} = (G_{ij})^{-1} = \begin{bmatrix} G^{11} & G^{12} \\ G^{21} & G^{22} \end{bmatrix} = A^{-1}A^{-T}$$

- A matrices and G's are all analytical, and can be pre-computed.

2D System: Shallow Water Model on the Cubed-Sphere

Flux-form SW equations (Vector invariant form):

[Nair, Thomas & Loft (MWR, 2005a,b)]

$$\begin{aligned}
\frac{\partial u_1}{\partial t} + \frac{\partial}{\partial x^1} E &= \sqrt{G}\, u^2 (f + \zeta) \\
\frac{\partial u_2}{\partial t} + \frac{\partial}{\partial x^2} E &= -\sqrt{G}\, u^1 (f + \zeta) \\
\frac{\partial}{\partial t}(\sqrt{G}\, h) + \frac{\partial}{\partial x^1}(\sqrt{G}\, u^1 h) + \frac{\partial}{\partial x^2}(\sqrt{G}\, u^2 h) &= 0
\end{aligned}$$

where $G = \det(G_{ij})$, h is the height, f Coriolis term; energy term and vorticity are defined as

$$E = \Phi + \frac{1}{2}(u_1\, u^1 + u_2\, u^2),\ \zeta = \frac{1}{\sqrt{G}} \left[\frac{\partial u_2}{\partial x^1} - \frac{\partial u_1}{\partial x^2} \right].$$

HOMME (DG) SW Model Discretization

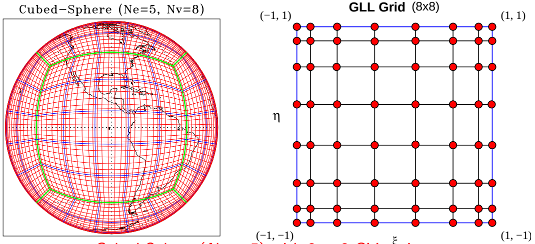

Cubed-Sphere ($N_e = 5$) with 8×8 GLL points

- Each face of the cubed-sphere is partitioned into $N_e \times N_e$ rectangular non-overlapping elements (i.e., total $6 \times N_e^2$ spans the entire sphere).
- Each element is mapped onto the Gauss-Lobatto-Legendre (GLL) grid defined by $-1 \leq \xi, \eta \leq 1$, for integration.
- Flux is the only "communicator" at the element edges. Nearest neighbor communication is ideal for parallel implementation.

SW Model: Advection of a Cosine-bell [Williamson et al., 1992]

- The DG transport is more accurate than the SE transport *[Nair et al. 2005]*

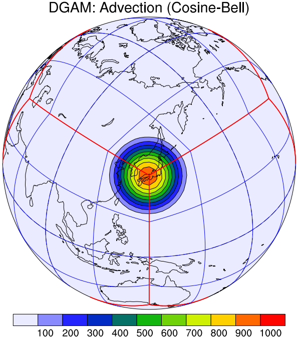

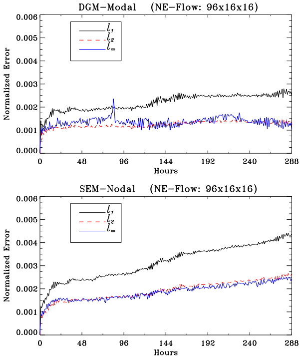

DGM Vs SEM run: Time traces for the normalized ℓ_1,ℓ_2 and ℓ_∞ errors ($\Delta t = 30s$)

Cosine-Bell Movie

DG SW Model: Advection Tests

- Global Transport with the monotonic limiter

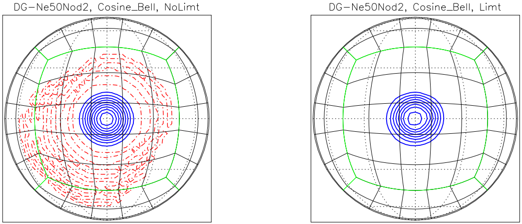

- Spectral convergence with a Gaussian-hill advection on the sphere

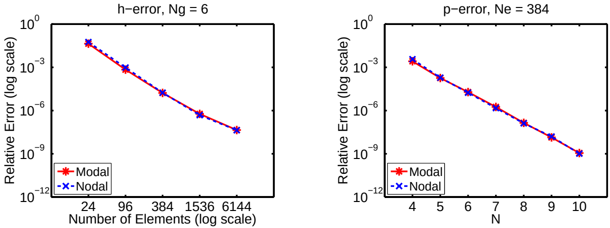

Low-Order Tests: Second-Order DG Vs FV-MUSCL

- Strong curvature terms associated with cubed-sphere geometry creates difficulty for the regular FV transport schemes

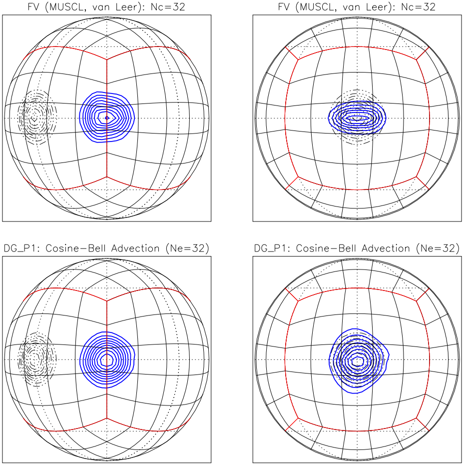

Cosine-Bell advection along the equator

Advection: Deformational Flow (Moving Vortices on the Sphere)

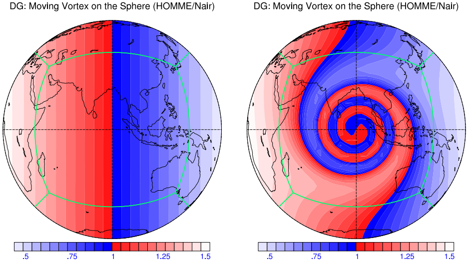

Initial field and DG solution after 12 days. Max error is $\mathcal{O}(10^{-5})$

A New Deformational Flow Test *[Nair & Jablonowski (MWR, 2008)]*

- The vortices are located at diametrically opposite sides of the sphere, the vortices deform as they move along a prescribed trajectory.
- Analytical solution is known and the trajectory is chosen to be a great circle along the NE direction ($\alpha = \pi/4$).

SW Test-2: Geostrophic Flow *[Nair, Thomas & Loft, MWR 2005]*

- High-order accuracy and spectral convergence

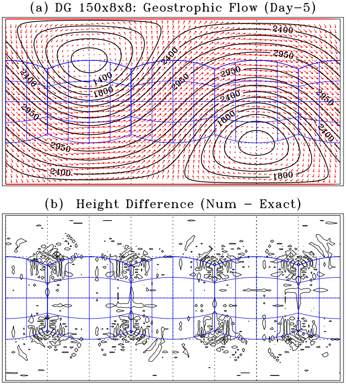

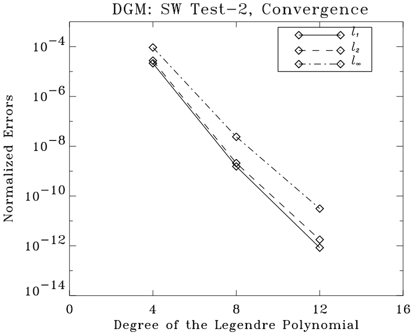

Steady state geostrophic flow ($\alpha = \pi/4$). Max height error is $\mathcal{O}(10^{-6})$ m.

SW Test-5: Flow over a Mountain [Dennis et al. 2006]

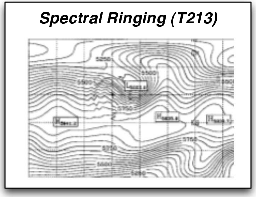

- "Spectral ringing" (spurious oscillation) is associated with the high-order spectral methods (Jacob-Chien et al., 1995)
- No spectral ringing for the height fields in DG simulations

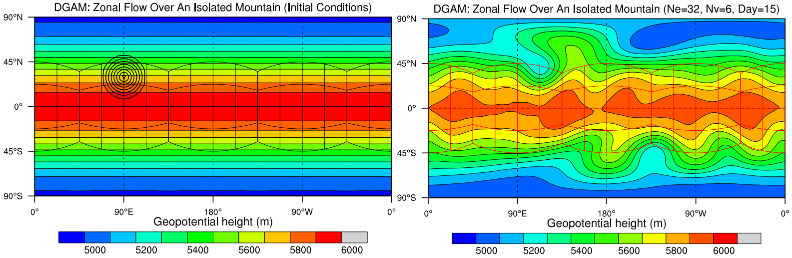

Flow over a mountain ($\approx 0.5^o$). Initial height field (left) initial and after 15 days of integration (right)

SW5 Movie

Viscous Shallow Water Model on the Cubed-Sphere

Local Discontinuous Galerkin (LDG) method: *[Bassi and Rebay (JCP, 1997]*

- Element-wise localized diffusion (ELD) leads to inconsistent formation of diffusion (viscous flux) terms in DG discretization.

Momentum equations for viscous SW model can be written in the following general form:

$$\frac{\partial}{\partial t} U + \nabla_c \cdot \mathbf{F}(U) = \nu \sqrt{G}\, \nabla_s^2\, U + S(U), \quad \text{in} \quad \mathcal{C} \times (0, T],$$

where ν is the diffusion coefficient, $\mathbf{F} = (F_1, F_2)$ is the flux function, and $\nabla_c \equiv (\partial/\partial x^1, \partial/\partial x^2)$.

$$\begin{aligned} \sqrt{G}\, \nabla_s^2 U &\equiv \sqrt{G}\, \mathrm{div}(\mathrm{grad}(U)) \\ &= \frac{\partial}{\partial x^1} \left[\sqrt{G} G^{11} \frac{\partial U}{\partial x^1} + \sqrt{G} G^{12} \frac{\partial U}{\partial x^2} \right] + \frac{\partial}{\partial x^2} \left[\sqrt{G} G^{21} \frac{\partial U}{\partial x^1} + \sqrt{G} G^{22} \frac{\partial U}{\partial x^2} \right]. \end{aligned}$$

Viscous Shallow Water Model on the Cubed-Sphere

- The key idea of LDG approach is the introduction of a local auxiliary variable $\mathbf{q} = \nabla_c U$, and rewrite the momentum equation as a first-order system:

$$
\begin{aligned}
\mathbf{q} - \nabla_c U &= 0, \\
\widetilde{\mathbf{q}} &= \mathbf{q}\,\mathbf{M}^T, \\
\frac{\partial U}{\partial t} + \nabla_c \cdot \mathbf{F}(U) - \nu\, \nabla_c \cdot \widetilde{\mathbf{q}} &= S(U).
\end{aligned}
$$

Where

$$
\mathbf{q} = \left[\frac{\partial U}{\partial x^1}, \frac{\partial U}{\partial x^2} \right], \quad \mathbf{M} = \begin{bmatrix} \sqrt{G}G^{11} & \sqrt{G}G^{12} \\ \sqrt{G}G^{21} & \sqrt{G}G^{22} \end{bmatrix} \quad \text{and} \quad \widetilde{\mathbf{q}} = \mathbf{q}\,\mathbf{M}^T.
$$

- On each element Ω_e with boundary Γ_e on $\mathcal{C}$, the weak form results in

$$
\int_{\Omega_e} \mathbf{q}_h \cdot \mathbf{w}\, d\Omega = \int_{\Gamma_e} U_h\, \mathbf{w} \cdot \mathbf{n}\, d\Gamma - \int_{\Omega_e} U_h \nabla_c \cdot \mathbf{w}\, d\Omega
$$

- The flux associated with U_h along the boundary Γ_e is approximated with the central flux

Diffusion Experiments: ELD Vs LDG *[Nair, MWR 2009]*

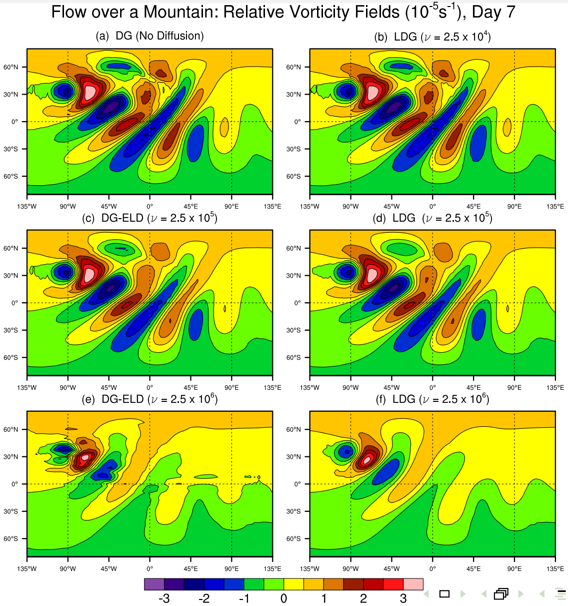

Diffusion Experiments: Barotropic Instability Test *[Galewsky, Tellus 2004]*

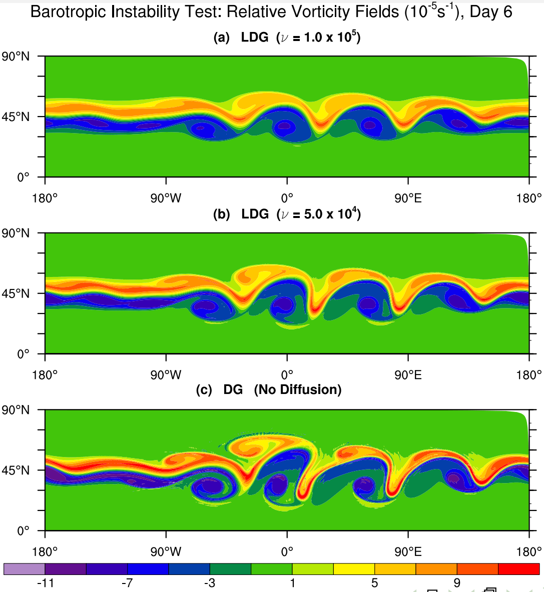

3D DG Hydrostatic Model in HOMME

- Extending the DG SW model to a hydrostatic dynamical core:
  - The DG hydrostatic model is a conservative option in the HOMME (High-Order Method Modeling Environment) framework
  - Vertical coordinates are Lagrangian and based on 'evolve and remap' strategy
  - The 3D hydrostatic atmosphere can be treated as a vertically stacked shallow water systems
  - Periodic remapping is performed with a conservative method

Hydrostatic Prognostic Equations in Flux Form (Curvilinear coordinates)

$$
\begin{aligned}
\frac{\partial u_1}{\partial t} + \nabla_c \cdot \mathbf{E}_1 + \dot{\eta}\frac{\partial u_1}{\partial \eta} &= \sqrt{G}u^2\,(f+\zeta) - R\,T\frac{\partial}{\partial x^1}(\ln p) \\
\frac{\partial u_2}{\partial t} + \nabla_c \cdot \mathbf{E}_2 + \dot{\eta}\frac{\partial u_2}{\partial \eta} &= -\sqrt{G}u^1\,(f+\zeta) - R\,T\frac{\partial}{\partial x^2}(\ln p) \\
\frac{\partial}{\partial t}(m) + \nabla_c \cdot \left(\mathbf{U}^i\, m\right) + \frac{\partial(m\dot{\eta})}{\partial \eta} &= 0 \\
\frac{\partial}{\partial t}(m\Theta) + \nabla_c \cdot \left(\mathbf{U}^i\,\Theta\, m\right) + \frac{\partial(m\dot{\eta}\,\Theta)}{\partial \eta} &= 0 \\
\frac{\partial}{\partial t}(mq) + \nabla_c \cdot \left(\mathbf{U}^i\, q\, m\right) + \frac{\partial(m\dot{\eta}\, q)}{\partial \eta} &= 0
\end{aligned}
$$

$$
m \equiv \sqrt{G}\,\frac{\partial p}{\partial \eta}, \nabla_c \equiv \left(\frac{\partial}{\partial x^1}, \frac{\partial}{\partial x^2}\right),\ \eta = \eta(p, p_s),\ G = \det(G_{ij}),\ \frac{\partial \Phi}{\partial \eta} = -\frac{R\,T}{p}\,\frac{\partial p}{\partial \eta}.
$$

Where m is the mass function, Θ is the potential temperature and q is the moisture variable. $\mathbf{U}^i = (u^1, u^2)$, $\mathbf{E}_1 = (E, 0)$, $\mathbf{E}_2 = (0, E)$; $E = \Phi + \frac{1}{2}\left(u_1 u^1 + u_2 u^2\right)$ is the energy term. Φ is the geopotential, ζ is the relative vorticity, and f is the Coriolis term.

Vertical Lagrangian Coordinates *[Starr, 1945; Lin 2004; Nair & Tufo 2007]*

A "vanishing trick" for vertical advection terms

- Terrain-following Eulerian surfaces are treated as material surfaces.
- The resulting Lagrangian surfaces are free to move up or down direction.

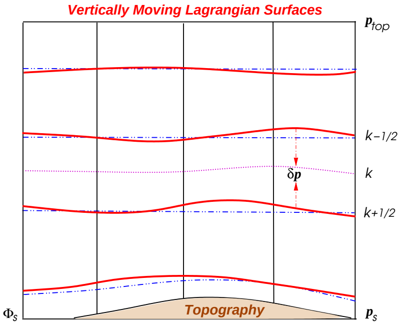

3D Prognostic Equations with Vertical Lagrangian Coordinates

- Lagrangian treatment of the Vertical coordinates results in $\dot{\eta} = 0$ and the mass function $m = \sqrt{G}\delta p = \Delta p$ (pressure thickness).
- Contravariant formulation preserves the familiar "vector invariant" form for the momentum equations.

Momentum Equations: No explicit vertical advection terms

$$
\begin{aligned}
\frac{\partial u_1}{\partial t} + \nabla_c \cdot \mathbf{E}_1 &= \sqrt{G}u^2\,(f + \zeta) - R\,T\frac{\partial}{\partial x^1}(\ln p) \\
\frac{\partial u_2}{\partial t} + \nabla_c \cdot \mathbf{E}_2 &= -\sqrt{G}u^1\,(f + \zeta) - R\,T\frac{\partial}{\partial x^2}(\ln p)
\end{aligned}
$$

$$\nabla_c \equiv \left(\frac{\partial}{\partial x^1}, \frac{\partial}{\partial x^2}\right), \quad \mathbf{E}_1 = (E, 0),\ \mathbf{E}_2 = (0, E),$$

$$E = \Phi + \frac{1}{2}\left(u_1 u^1 + u_2 u^2\right)$$

3D Prognostic Equations: Flux-Form Continuity Equations

Temperature field is advected with the mass variable Δp

$$\frac{\partial}{\partial t}(\Delta p) + \nabla_c \cdot \left(\mathbf{U}^i\, \Delta p\right) = 0$$
$$\frac{\partial}{\partial t}(\Theta \Delta p) + \nabla_c \cdot \left(\mathbf{U}^i\, \Theta\, \Delta p\right) = 0$$
$$\frac{\partial}{\partial t}(q\, \Delta p) + \nabla_c \cdot \left(\mathbf{U}^i\, q\, \Delta p\right) = 0$$

where $\mathbf{U}^i = \left(u^1, u^2\right)$, $\Delta p = \sqrt{G}\delta p$, δp is the pressure thickness, and Θ is the potential temperature.

Vertical layers are coupled with the hydrostatic relations:

$$\Delta\Phi = -C_p \Theta \Delta\Pi, \quad \Delta\Phi = -RT\Delta \ln p$$

where $\Pi = (p/p_0)^\kappa$ and T Denotes the layer mean temperature.

The Remapping of Lagrangian Variables

Vertically moving Lagrangian Surfaces

- Over time, Lagrangian surfaces deform and thus must be remapped.
- The velocity fields (u_1, u_2), and total energy (Γ_E) are remapped onto the reference coordinates using the 1-D conservative cell-integrated semi-Lagrangian (CISL) method (*Nair & Machenhauer, 2002*)

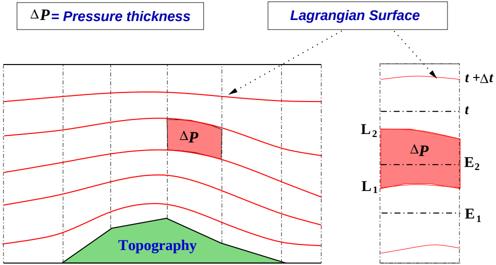

Terrain–following Lagrangian control–volume coordinates

Remapping: Lauritzen & Nair, MWR, 2008; Norman & Nair, MWR, 2008)

Computational Grid Structure for DG Model

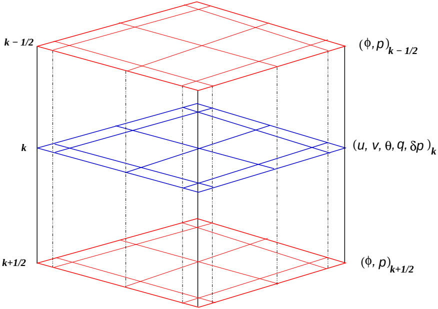

GLL− Grid box

- The remapping frequency is $\mathcal{O}(10) \times \Delta t$
- Potential temperature Θ is retrieved from the remapped total energy $\Gamma_E = c_p T + \frac{\delta(p\phi)}{\delta p} + K_E$

DG-3D: Baroclinic Instability Test

JW-Test *[Jablonowski & Williamson* (QJRMS, 2006)]

- A standard benchmark test for atmospheric dynamical cores
- To assess the evolution of an idealized baroclinic wave in the Northern Hemisphere.
- The initial conditions are quasi-realistic and defined by analytic expressions. Analytic solutions do not exist.

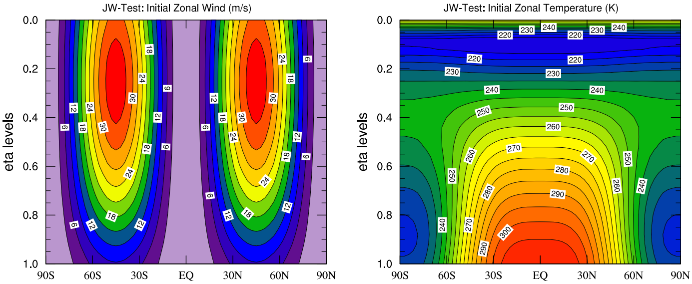

Initial Conditions

JW-Test: Evolution of Surface Pressure over the NH

- Baroclinic waves are triggered by perturbing the velocity field at (20°E, 40°N)
- This test case recommends up to 30 days of model simulation
- Ne = Nv = 8 (approx. 1.6°) with 26 vertical levels and $\Delta t = 30$ Sec.

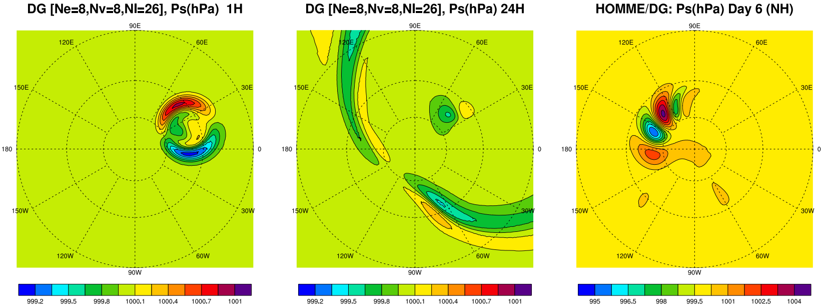

DG-3D Model Vs. NCAR Spectral Model

- The DG Solution is smooth and free from "spectral ringing".

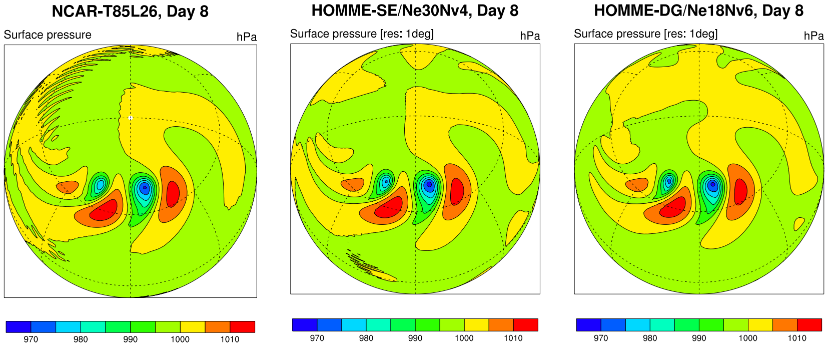

DG Model Vs. NCAR Climate Models *[Nair, Choi & Tufo, 2009]*

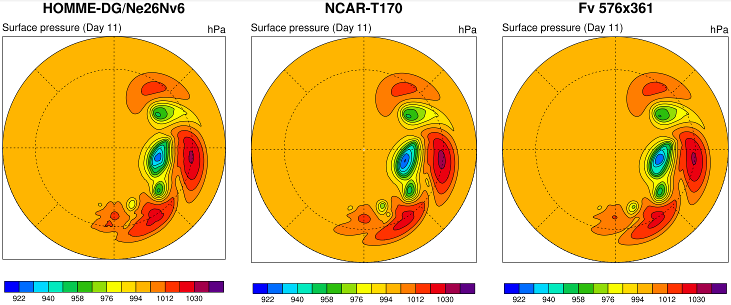

Simulated surface pressure at day 11 for a baroclinic instability test with DG model, NCAR spectral & FV models

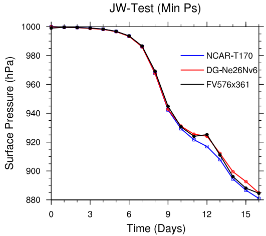

DG-3D Model Vs. Other Models

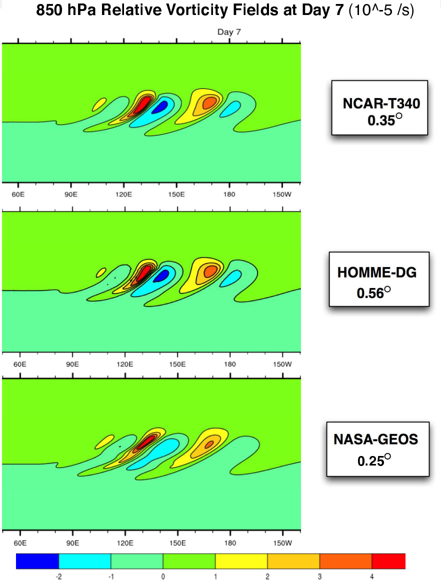

DG-3D Model Vs. NCAR Climate Models

Temperature fields at 850 hPa level, with HOMME-DG, NCAR Spectral & FV models.

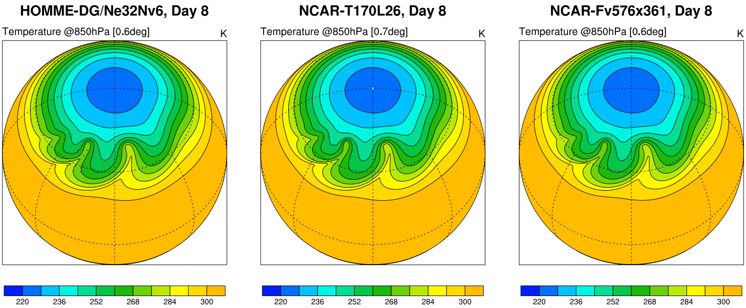

- The DG-3D model successfully simulates the Baroclinic instability and the results are comparable with that of the NCAR models.

Parallel Performance (3D) - Frost [IBM BG/L]

- DG-3D parallel performance: Sustained Mflops on IBM BG/L (1024 DP nodes, 700 MHz PPC 440s): Approx. 9% peak (preliminary results without code optimization)

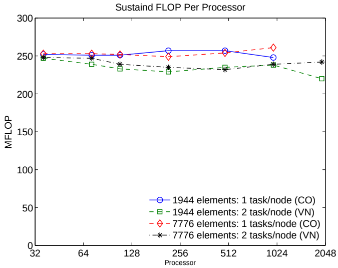

- HOMME-DG dynamical core employs 6th order polynomials and about 50% slower than the HOMME-SE dynamical core (with 4th order polynomials).
- However, a third-order DG version in HOMME (CFL ≈ 0.21) can compensate the integration rate deficiency

- Idealized climate simulations (Held-Suarez, aqua planet) with CAM/HOMME-SE dynamical core (Taylor et al. 2008) is very promising. Integration of HOMME-DG with CAM physics is an ongoing effort.

Summary

- The DG method with moderate order (third or fourth) is an excellent choice for solving conservation laws as applied in atmospheric sciences. DGM addresses:
  1. Local and global conservation
  2. High-order accuracy
  3. Geometric flexibility
  4. Non-oscillatory advection
  5. High parallel efficiency
- Non-oscillatory DG transport (positive definite option) is found to be accurate and effective up to third-order.
- The preliminary idealized test results and parallel scaling results are impressive and comparable to the SE version in HOMME.
- The LDG formulation is consistent and very effective for diffusion mechanism in HOMME/DG
- The explicit Runge-Kutta time integration scheme is robust for the DG-3D model, but very time-step restrictive.

Future Work

- Coupling HOMME-DG with the CAM/CCSM *physics* for the *real* climate simulations. Targeting for large-scale parallelism with $\mathcal{O}(100K)$ processors.
- Efficient time stepping
  - More efficient time integration schemes are required for practical application climate simulations.
  - Possible approaches: Semi-implicit, implicit, IMEX-RK, Rosenbrock with optimized Schwarz, etc.. (supported by the DOE SciDAC project)
- Extending HOMME further to a full Non-Hydrostatic model
  - Tools: Third-order DG combined with non-oscillatory H-WENO method; efficient FV methods

THANK YOU!

Ram Nair
Institute for Mathematics applied to Geosciences
National Center for Atmospheric Research
Table Mesa Drive, Boulder CO 80305, USA.
rnair@ucar.edu
http://www.image.ucar.edu/staff/rnair/

NCAR